

The ovipositor actuation mechanism of a parasitic wasp and its functional implications

Noraly M. M. E. van Meer¹  | Uroš Cerkvnik¹  | Christian M. Schlepütz²  |
Johan L. van Leeuwen¹  | Sander W. S. Gussekloo¹ 

¹Experimental Zoology Group, Wageningen University, Wageningen, The Netherlands

²Swiss Light Source, Paul Scherrer Institute, Villigen, Switzerland

Microfluidics Lab, Department of Aerospace and Mechanical Engineering, University of Liège, Liège, Belgium
Functional and Evolutionary Morphology Laboratory, FOCUS, University of Liège, Liège, Belgium

Correspondence

Sander W.S. Gussekloo, Experimental Zoology Group, Wageningen University, De Elst 1, 6708 Wageningen, The Netherlands
Email: sander.gussekloo@wur.nl

Funding information

Stichting voor de Technische Wetenschappen, Grant/Award Number: STW12712

Abstract

Parasitic wasps use specialized needle-like structures, ovipositors, to drill into substrates to reach hidden hosts. The external ovipositor (tereбра) consists of three interconnected, sliding elements (valvulae), which are moved reciprocally during insertion. This presumably reduces the required pushing force on the tereбра and limits the risk of damage whilst probing. Although this is an important mechanism, it is still not completely understood how the actuation of the valvulae is achieved, and it has only been studied with the ovipositor in rest position. Additionally, very little is known about the magnitude of the forces generated during probing. We used synchrotron X-ray microtomography to reconstruct the actuation mechanism of the parasitic wasp *Diachasmimorpha longicaudata* (Braconidae) in four distinct phases of the probing cycle. We show that only the paired first valvulae of the tereбра move independently, while the second valvula moves with the metasoma ('abdomen'). The first valvula movements are initiated by rotation of one chitin plate (first valvifer) with respect to another such plate (second valvifer). This is achieved indirectly by muscles connecting the non-rotating second valvifer and the abdominal ninth tergite. Contrary to previous reports, we found muscle fibres running inside the tereбра, although their function remains unclear. The estimated maximal forces that can be exerted by the first valvulae are small (protraction 1.19 mN and retraction 0.874 mN), which reduces the risk of buckling, but are sufficient for successful probing. The small net forces of the valvulae on the substrate may still lead to buckling of the tereбра; we show that the sheaths surrounding the valvulae prevent this by effectively increasing the diameter and second moment of area of the tereбра. Our findings improve the comprehension of hymenopteran probing mechanisms, the function of the associated muscles, and the forces and damage-limiting mechanism that are involved in drilling a slender tereбра into a substrate.

KEYWORDS

hymenoptera, kinematics, musculature, ovipositor, synchrotron X-ray micro-computed tomography

This is an open access article under the terms of the Creative Commons Attribution-NonCommercial-NoDerivs License, which permits use and distribution in any medium, provided the original work is properly cited, the use is non-commercial and no modifications or adaptations are made.

© 2020 The Authors. *Journal of Anatomy* published by John Wiley & Sons Ltd on behalf of Anatomical Society

1 | Introduction

Reproduction is one of the most important elements in the life history of animals. In many species, we therefore see behaviours and morphological adaptations that increase reproductive success. Many insects, for example, hide their eggs in substrates that provide food and protection for the developing larvae (Zeh *et al.* 1989). Many parasitic wasps take advantage of that and lay their eggs in the larvae of host species that are already hidden deep within substrates such as fruits and wood (Heatwole *et al.* 2010; Ghara *et al.* 2011; Elias *et al.* 2012). To reach these hosts, wasps drill into the substrate with a long and thin (slender) external ovipositor or terebra (Fig. 1A; Kundanati and Gundiah, 2014; Cerkvénik *et al.* 2017). Not only can these animals penetrate the often stiff substrates, but they can also steer their terebrae to reach the desired targets (Elias *et al.* 2012; Cerkvénik *et al.* 2017). This probing behaviour is a challenging task as slender drilling structures can easily buckle and become damaged as a result of substrate reaction forces (King and Vincent, 1995; Kundanati and Gundiah, 2014; Sakes *et al.* 2016).

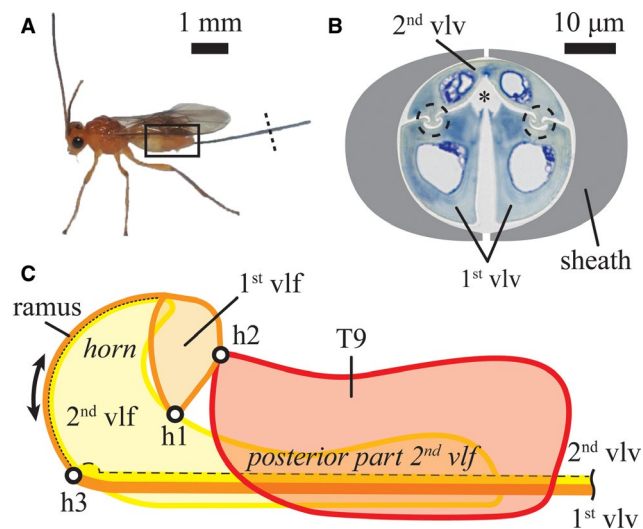


FIG. 1 Ovipositor apparatus of a parasitic wasp. (A) Parasitic wasp *Diachasmimorpha longicaudata*. The dotted line roughly indicates the location of the transverse section through the ovipositor shown in panel B and the rectangle roughly indicates the location of the ovipositor apparatus shown in panel C. (B) A schematic cross-section of the ovipositor of *D. longicaudata* (at dashed line in A). Black dashed circles indicate the interlocking olistheter mechanism. Asterisk indicates the egg canal. 'Sheath' refers to sheaths surrounding the ovipositor. (C) Schematic representation of the left side of the apocritan ovipositor apparatus (based on Fergusson, 1988). All elements have a mirror image on the right side, apart from the second valvula (2nd vlv), which is a single bilateral symmetric element located in the median. The second valvifer (2nd vlv) consists of an anterior horn and a posterior rectangular part. It is connected to the 2nd vlv. The first valvifer (1st vlv) is continuous with the first valvula (1st vlv) via a ramus. The 1st vlv hinges on the 2nd vlv at hinge h1 and with the ninth abdominal tergite (T9) at h2. The external ovipositor can rotate in the medial plane around h3. [Colour figure can be viewed at wileyonlinelibrary.com]

However, parasitic wasps clearly avoid damaging the terebra, as most wasps lay eggs in multiple drilling sessions throughout their life (Godfray, 1994). A good understanding of how parasitic wasps avoid damage to their ovipositors, and how they drill into and steer within often tough substrates is relevant in many aspects as it provides insight into the adaptation and co-evolution occurring in the group of Hymenoptera.

To fully understand the working mechanism of the ovipositor, a solid knowledge of its morphology is essential. The insect terebra originally consisted of four elements: two ventral valvulae (also called 'first valvulae') and two dorsal valvulae (also called 'second valvulae'), but fusion of elements occurred during evolution in various insect taxa (Imms, 1931). In parasitic wasps, the two second valvulae are generally merged, which results in terebrae with three functional elements (Fig. 1B; Smith, 1970; Smith, 1972; Quicke *et al.* 1994). The first and second valvulae are longitudinally interconnected with a tongue-and-groove (olistheter) mechanism that allows longitudinal sliding of the elements, while preventing their separation (Fig. 1B; Smith, 1969; Quicke *et al.* 1994; Scudder, 2009). It has been hypothesized that during probing many insects move these valvulae in saw-like fashion (Smith, 1969; Quicke *et al.* 1994; King and Vincent, 1995), which has recently been confirmed for the parasitic wasp *Diachasmimorpha longicaudata* Ashmead (Braconidae; Cerkvénik *et al.* 2017). The alternating movements of the valvulae are thought to play an important role in buckling avoidance as they facilitate the so-called push-pull mechanism (King and Vincent, 1995).

According to this mechanism, buckling is avoided by pushing only certain valvulae, while simultaneously pulling on others that are fixed in the substrate (King and Vincent, 1995; Sakes *et al.* 2016). The tension in the latter valvulae increases their flexural stiffness, which allows them to serve as guides for the valvulae that are pushed into the substrate (King and Vincent, 1995). The reciprocal movements appear crucial for penetration of solid substrates, particularly when dealing with stiff substrates, as was shown for the parasitic wasp *D. longicaudata*. This species always uses the reciprocal mechanism to insert the terebra in stiff substrates, but not in softer ones (Cerkvénik *et al.* 2017).

In addition to simplifying insertion in stiff substrates, it has also been hypothesized that the movement of individual valvulae plays an important role in steering the probe (Quicke, 1991; Quicke *et al.* 1995; Quicke and Fitton, 1995; Cerkvénik *et al.* 2017). In *D. longicaudata*, the predominant protraction of the first valvula leads to curved trajectories, while predominant protraction of the second valvula leads to straight insertions (Cerkvénik *et al.* 2017). This shows how important accurate actuation of the valvulae for successful egg deposition is. Although knowledge regarding the kinematics of the valvulae, and the morphology of the muscles that actuate them is increasing, the movements of the actuation system are currently only hypothesized and have never been visualized or analysed. Knowledge of the amplitude of the movements of the valvulae and the magnitude of the forces that can be exerted by the animals will provide insight into maximal performance and better understanding of the drilling mechanism.

Current knowledge about the functioning of the ovipositor apparatus is solely based on morphological descriptions of dead specimens in resting position, with the terebra close to the metasoma ('abdomen') pointing backwards (e.g. King, 1962; Fergusson, 1988; Copland and King, 2009). From these and other descriptions (Imms, 1931; Smith, 1970; Scudder, 1971; Smith, 1972; Quicke *et al.* 1994; Scudder, 2009; Copland and King, 2009; Eggs *et al.* 2018) it is clear that the muscles that move the valvulae are positioned inside the abdomen, at the base of the valvulae. Inside the abdomen, the valvulae attach to plate-like basal sclerites (valvifers) that evolved from the coxae of the eighth and ninth abdominal segments (Imms, 1931; Smith, 1970; Scudder, 2009; Copland and King, 2009; Chapman, 2013; Eggs *et al.* 2018). The valvifer shapes, arrangements, and articulations differ across insect species (Scudder, 1971; Scudder, 2009; Klass *et al.* 2012), but are comparable across hymenopterans (Fig. 1C; Imms, 1931; Smith, 1970; Copland, 1976; Fergusson, 1988; Vilhelmsen, 2000; Eggs *et al.* 2018). The first valvulae attach via long rami to the usually triangular first valvifers (Smith, 1970), while the fused second valvula attaches via smaller rami to two large second valvifers (Imms, 1931). The first valvulae and their rami bear the aulaces (grooves) of the olistheter mechanism, whereas the second valvula and the anterior ridges of the second valvifers bear the rhachises (ridges; Scudder, 2009). The second valvifers often bear at their posterior ends a pair of ovipositor sheaths (third valvulae) that envelop the terebra in the rest position and may help to stabilize the terebra during probing (Fig. 1B; Vilhelmsen, 2003; Cerkvenik *et al.* 2017). The first and second valvifers are linked with a hinge that allows rotation of the first valvifer [intervalvifer articulation; hinge 1 (h1) in Fig. 1C; Imms, 1931; Smith, 1970; Eggs *et al.* 2018]. A second hinge is present between the first valvifer and the ninth tergite (T9) of the abdomen (tergo-valvifer articulation; h2 in Fig. 1C; Smith, 1970; Scudder, 2009; Eggs *et al.* 2018). A third, harder to recognize, hinge (basal articulation) is located at the base of the second valvula and allows rotation of the terebra in the medial plane (h3 in Fig. 1C).

During probing, the ovipositor is rotated downward into probing position (Cerkvenik *et al.* 2017), which presumably results in significant changes in the configuration of the basal elements of the ovipositor. It is therefore not certain how any of the elements move during probing, apart from the sliding motion of the valvulae, which has recently been visualized and quantified (Cerkvenik *et al.* 2017). The existing consensus is that the external ovipositor as a whole can be pivoted downwards around hinge 3 (h3) to get it into probing position. Protraction of the first valvulae is achieved by rotation of the first valvifer, which in turn is induced by pulling the second valvifers and T9 closer together. Retraction of the first valvulae is achieved by moving the second valvifers and T9 further apart (Smith, 1969; Fergusson, 1988; Eggs *et al.* 2018). This movement pattern is, however, completely theoretical and has never been recorded or quantified.

Analysing the actuation mechanism of the ovipositor is a major challenge. Visualization of the kinematics of the ovipositor base

in vivo is extremely difficult, because it is hidden inside the abdomen and is very small in most species. As mentioned, existing studies only describe the system with the ovipositor in resting position, which may be strikingly different from the probing situation. Furthermore, the relative positions and orientations of the valvifers and the T9 have not been quantified, and there are currently no data on the force production of the ovipositor base musculature. To our knowledge, only one instance exists where the researchers determined the physiological cross-sectional areas (PCSAs) of the muscles as an indication for muscle force (Eggs *et al.* 2018).

In the present study, we focus on the functional aspects of a number of these issues by analysing the ovipositor apparatus of the parasitic wasp *D. longicaudata*, for which the valvula kinematics have been quantified (Cerkvenik *et al.* 2017). We used high-resolution synchrotron X-ray microtomography and 3D anatomical analysis to determine the configuration of the probing apparatus in different phases of the probing cycle. This allowed us to derive the kinematics of the complete probing cycle and to calculate the range of motions of the valvifers and the valvulae. We also measured the PCSA and the moment arms of the actuating muscles based on the position of their attachments. This allowed us to estimate the forces acting on the valvulae by assuming a particular tensile stress in the muscle fibres. As mentioned above, this brings novel insights into the maximal performance of these animals and their adaptations. In addition, it will add to the understanding of probing with slender structures, which may be applied in man-made probes.

2 | Materials and methods

2.1 | Animals

A total of nine animals of the species *D. longicaudata* were obtained from a colony maintained with the breeding protocol as previously described (Cerkvenik *et al.* 2017) at the Experimental Zoology Group at Wageningen University (Wageningen, the Netherlands).

2.2 | Body positions and valvula configurations

To recreate a full drilling cycle, we prepared wasps with the ovipositor in two body positions and three valvula configurations (Table 1): (a) in resting position with the valvulae aligned at the tips (aligned valvulae); (b) in probing configuration with aligned valvulae; (c) in probing configuration with retracted first valvulae; and (d) in probing configuration with protracted first valvulae.

To obtain the probing configurations, live parasitic wasps were offered a gel-filled cuvette containing a Mediterranean fruit fly larva (*Ceratitis capitata* Wiedemann) at the bottom (see Cerkvenik *et al.* 2017). After the wasps started probing and when the terebra was fully inserted into the substrate, the cuvette and the wasp were

TABLE 1 Overview of the animals and their treatments.

Valvula configuration	Resting position		Probing position	
	Aligned valvulae	Aligned valvulae	Retracted first valvulae	Protracted first valvulae
Achieved by	natural	adjusted	natural	adjusted
Preparation	decapitation ($n = 1$) liquid nitrogen ($n = 2$)	liquid nitrogen	liquid nitrogen	liquid nitrogen
Staining	IKI ^{a,b} , None ^{a,b}	I ₂ E ^{a,b}	IKI ^a	IKI ^a
Segmentation Software	Seg3D + MeVisLab, MeVisLab	Seg3D + MeVisLab	MeVisLab	MeVisLab

IKI, iodine-potassium-iodide.

^aSpecimen used for reconstruction of the exoskeletal elements.

^bSpecimen used for muscle reconstruction.

quickly submerged in liquid nitrogen to preserve the wasp's body shape and position. Preliminary analysis showed that in all cases this resulted in ovipositors with retracted first valvulae. To obtain the other phases of the probing cycle, we thawed the wasps and used fine tweezers to slide the valvulae into the desired configuration, while keeping the body position intact.

For the resting position, two wasps were placed inside a histology embedding cassette and frozen in liquid nitrogen, similar to the treatment of the probing animals. After the desired configuration was obtained the valvulae of all specimens were kept in place with a droplet of beeswax to preserve this configuration during the staining process (see below).

As a control for freezing, fixing, staining and drying effects in the treated specimen, a living wasp was decapitated, and scanned within minutes of decapitation with the ovipositor in resting position.

2.3 | Fixing and staining

All wasps, except for the control, were stained with iodine for increased contrast in the CT scans, according to either the iodine-potassium-iodide (IKI) or I₂E staining protocols (Metscher, 2009). In both protocols, the wasps were thawed for approximately 1 min at room temperature before fixing in Bouin's solution overnight. Afterwards, the head and mesosoma ('thorax') were cut off to facilitate the entry of the staining solution into the abdomen posterior to the wasp waist (metasoma). In the IKI protocol, the specimens were washed with 70% ethanol, and in three steps (50% and 30% ethanol) transferred to distilled water with 0.05% Tween20. The specimens were then stained in a 10% IKI solution according to (Metscher, 2009) for at least 7 days at 7°C. In the I₂E protocol, the specimens were transferred in four steps (80%, 90% and 98% ethanol) to 100% ethanol and then stained in an I₂E solution (1% I₂ in 100% ethanol) for at least 7 days at room temperature according to (Metscher, 2009). During staining, both IKI and I₂E solutions were refreshed at least once a day, but more often in the first day of staining. After staining, the samples were washed with distilled water and mounted on carbon fibre rods with beeswax to secure them on the rotation platform of the CT scanner. The staining affected the samples

differently and we selected the samples that showed the best tissue contrast for further analysis. The IKI staining was usually more successful, although for the probing position with aligned valvulae the I₂E stained sample was used (Table 1).

2.4 | Synchrotron X-ray micro-computed tomography

High-resolution micro-computed tomography scans were acquired at the TOMCAT beamline X02DA of the Swiss Light Source facility (Paul Scherrer Institute, Switzerland). The scans were carried out with 18 keV (control) and 11 keV (all other scans) monochromatic X-ray beams. Projection images were recorded over an angular range of 180°, with an angular step of 0.1° with a PCO Edge 5.5 sCMOS camera (exposure time of 100 ms), using a 20 µm thick LuAG:Ce scintillator. Whole metasoma scans were made at 20× magnification (resting configuration) and 10× magnification (probing configurations), resulting in effective pixel widths of 325 nm and 650 nm, respectively (Stampanoni *et al.* 2006). The scans were reconstructed using the 'gridrec' reconstruction algorithm (Marone and Stampanoni, 2012) together with propagation-based phase contrast (delta/beta ratio = 20) as described by Paganin *et al.* (2002).

2.5 | Analysis

2.5.1 | Segmentation

The reconstructed image stacks were processed with MeVisLab 2.8.2 (MeVis Medical Solutions AG). The contrast between tissues was increased using edge enhancement and by subtracting the original reconstruction from the edge-enhanced images. A rough segmentation was done by applying a simple threshold filter, such that all relevant structures were retained, while removing as many other structures as possible. This segmentation was improved by manually delineating the individual structures of interest at locations with low contrast. Finally, segmented elements were further improved by applying morphological dilation and erosion filters

which removed small artefacts and smoothed the outer boundaries of the elements (MeVisLab segmentation algorithm available on Dryad).

The tissue contrast in the unstained control wasps was low and only two muscles could be segmented using MeVisLab, and subsequently used for correction for staining and freezing artefacts. Two stained specimens showed low contrast and muscles were manually segmented using the 'paintbrush' function in Seg3D 2.2.1 [University of Utah (CIBC, 2016); Table 1] as this program offers more effective tools for manual segmentations than MeVisLab. All reconstructions were converted to polygon surface meshes for further visualization and measurements. For comparison between meshes, those from resting positions were positioned with the terebra in horizontal direction, while meshes of probing positions were aligned with the terebra in vertical direction.

2.5.2 | Maximal muscle force estimations

To obtain a rough estimate for the maximum forces that can be generated by the muscles moving the ovipositor and individual valvulae, we reconstructed the PCSA of these muscles. In our analysis, we omitted effects of muscle length change during contraction and other muscle characteristics that may affect force generation *in vivo*. As most muscles were nearly parallel-fibred (see Results) we used MeVisLab to manually orientate a plane through the widest part of the muscle reconstruction, perpendicular to the general direction of the muscle fibres. We used the combined cross-sectional area of the muscle fibres in this plane as a proxy for the PCSA.

To enable comparisons between individual wasps, we scaled all measurements to the dimensions of the control wasp. In the scaling, we assumed that chitin elements of the exoskeleton would not be affected by either staining or freezing, and scaled all reconstructions to the distance between easily identifiable landmarks on the second valvifer (for details see Supporting Information). Effects of freezing and staining were estimated based on the difference between the control and stained specimen in estimated cross-sectional area after size correction of two muscles (for details see Supporting Information).

The maximal muscle-force production was estimated by multiplying the cross-sectional area with a specific muscle tension. Specific muscle tensions of abdominal musculature are currently missing in the literature, so we reviewed previous data provided by Rospars and Meyer-Vernet (2016). From this dataset, we selected all insect muscles, with the exception of jumping or flying muscles because these are probably highly adapted for fast contraction speed or high force production. Two values remained, obtained from the femoral rotator muscle of the hind leg in the click beetle [*Carabus problematicus*; 210 kPa; (Evans, 2009)] and the mandible closer muscles of the male stag beetle [*Cyclommatus metallifer*; 180 kPa; (Goyens *et al.* 2014)]. We used the average of these muscles (195 kPa) as the estimation for the specific muscle tension for the muscles in the abdomen.

2.5.3 | Torques and forces on the exoskeletal elements

For the probing position with aligned valvulae, we determined the 3D orientations of rotation axes and positions of muscle attachment sites in the meshes of the reconstructed exoskeleton using MeshLab 1.3.2 (Cignoni *et al.* 2008). A custom MatLab (R2016b) script was used to calculate the muscle moment arms (r) from these coordinates. The maximal torques (M) exerted by the muscles on the ovipositor or the first valvifer were estimated using the scalar version of the torque equation: $M_i = r_i * F_i$, where r_i is the moment arm of muscle i with respect to the associated rotation axis and F_i the estimated maximal force of muscle i . Changes in moment arms during contraction were estimated based on the known distance of muscle insertions to the relative rotation point, and observed range of rotation from fully protracted to fully retracted.

The push and pull forces of the first valvula, exerted on the substrate, were estimated by dividing the sum of the maximal torques on the first valvifer with the average moment arm of the first valvulae (average of column r in Table 3), using the same torque formula as above.

3 | Results

3.1 | General morphology of the exoskeletal elements

The general morphology of the ovipositor basal apparatus is similar to that of previously described species (e.g. Imms, 1931; Smith, 1970; Scudder, 1971; Scudder, 2009; Ernst *et al.* 2013; Eggs *et al.* 2018). Because of its bilateral symmetry, we will only present data for one side of the animals. For the description of the anatomical structures, we follow the terminology of the Hymenoptera Anatomy Ontology Project (HymAO; Yoder *et al.* 2010). If terminology is used that is not in the HymAO, we will state this in the text.

The whole ovipositor apparatus is attached to the abdomen via the tergite of the ninth abdominal segment (T9). This tergite articulates with a small triangular element (first valvifer) which is continuous with the dorsal ramus of the first or ventral valvula (Fig. 2). The tergo-valvifer articulation (h2; Fig. 2B,E) between T9 and the first valvifer seems strong and allows rotation in the sagittal plane. Ventrally (in resting position), the first valvifer articulates with a larger plate-like element, the second valvifer (Fig. 2B,E). This inter-valvifer articulation (h1) allows rotation in the sagittal plane as well. The second valvifer consists roughly of two regions: an approximately rectangular posterior part and an anterior horn area. The second valvifer and T9 lie closely together, but do not touch (Fig. 2).

The needle-like external ovipositor or terebra is approximately 4.0 mm long and consists of three elements: one second valvula, and two first valvulae. The paired first valvulae are connected to the second valvula via an olistheter mechanism that consists of a rail-like tongue (rhachis) on the second valvula and a groove (aulax)

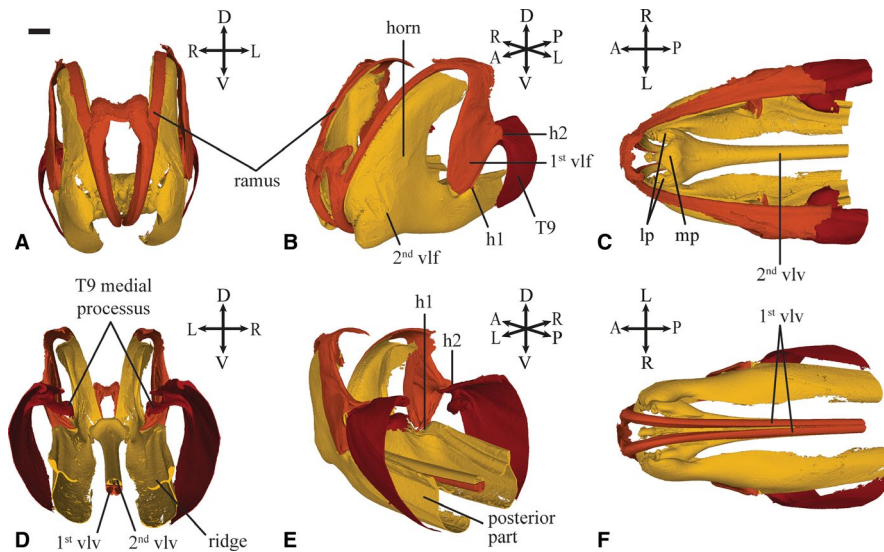


FIG. 2 Three-dimensional reconstruction of the ovipositor base of *Diachasmimorpha longicaudata* in resting position with aligned valvulae. The colours indicate different exoskeletal elements. Orange: first valvulae (1st vlv) and first valvifers (1st vlf); yellow: second valvula (2nd vlv) and second valvifers (2nd vlf); red: tergum 9 (T9). The orientation of the base in each image is indicated with arrows: anterior (A), posterior (P), dorsal (D), ventral (V), left (L), and right (R). (A) Anterior view showing the long rami connecting the 1st vlv with the 1st vlf running along the anterior ridge of the 2nd vlf. The medial connection is a thin membrane that does not affect independent movement. (B) Anterior-lateral view. (C) Dorsal view showing the enlargement (bulbus) of the 2nd vlv at its base, including the medial processus (mp) and two lateral processi (lp). (D) Posterior view showing the placement of the valvulae between the basal plates. (E) Posterior-lateral view. (F) Ventral view showing the 1st vlv. Scale bar: 100 μ m [Colour figure can be viewed at wileyonlinelibrary.com]

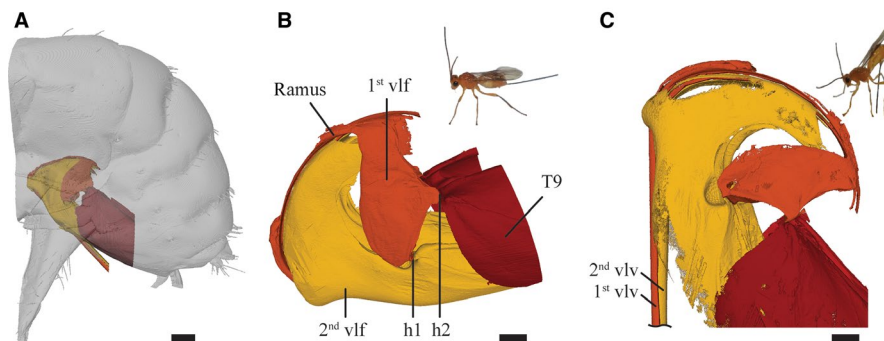


FIG. 3 Resting and probing positions of the ovipositor apparatus. (A) The ovipositor basal apparatus is located within the metasoma on its ventral side. Metasoma (grey) with the basal ovipositor (coloured) depicted in probing position with aligned valvulae. Distal part of the terebra not shown. (B) Top right: Wasp with ovipositor in resting position. Bottom: Side view of the configuration of the basal apparatus in the resting position with aligned valvulae; valvulae not shown. (C) Top right: Wasp in probing position. Bottom: Side view of the configuration of the basal apparatus in probing position. Scale bars: (A) 200 μ m, (B,C) 100 μ m for basal apparatus only, body length of wasp without ovipositor approximately 5 mm. See Fig. 2 for abbreviations [Colour figure can be viewed at wileyonlinelibrary.com]

in each of the first valvulae (Fig. 1B). This olistheter mechanism allows longitudinal sliding of the valvulae, but prevents separation of the elements. The first valvula extends anteriorly beyond the second valvula and forms an arched ramus with the aulax that runs along the anterior edge of the horn of the second valvifer. This anterior edge of the horn, like the second valvula, carries a rachis, which acts as an extension of the olistheter mechanism. The connecting ramus is a thin plate-like connection, and it is likely that flexion in this area occurs during the downward rotation of the terebra as observed during probing (Fig. 3C). The base of the second valvula is enlarged and divided into three processes: one medial and two lateral. The

first valvulae run below and in between these processes (Fig. 2). The egg canal runs in between the three valvulae (Fig. 1B).

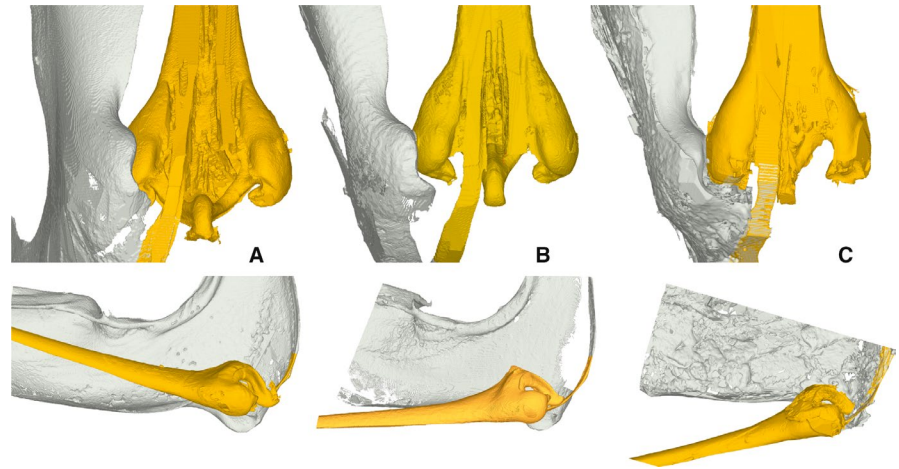
3.2 | Movements of the ovipositor basal apparatus

3.2.1 | From resting to probing position

Exoskeletal elements

When a wasp starts probing, it elevates its metasoma and rotates the terebra downwards and forwards away from its resting position

FIG. 4 Movement of the terebra base during depression. Top row: ventral view of the second valvula (yellow) and right second valvifer (grey), bottom row: medial view of the second valvula and right second valvifer. (A) Terebra in resting position. (B) Terebra in probing position 1. (C) Terebra in probing position 2 [Colour figure can be viewed at wileyonlinelibrary.com]



(Cerkvenik *et al.* 2017) (Fig. 3B,C). We will call this rotation terebra depression, and the opposite movement terebra elevation. Depression of the terebra is achieved by a straightening of the thin, short, rami of the first and second valvifer, in a small flexible area just behind the base of the terebra (Fig. 4). We refer to the rotation point as 'hinge 3' (h3) to avoid confusion about the term 'basal articulation' which has been used to describe the rotation point of the terebra, but at completely different locations (King, 1962; Smith, 1972; Copland, 1976; Fergusson, 1988; Copland *et al.* 2009). One of these locations was at the position of the lateral bulbs of the terebra base and the socket on the second valvifer (King, 1962; Copland, 1976; Fergusson, 1988; Copland *et al.* 2009). We observed that during terebra depression the lateral bulbi of the terebra were pulled out of the sockets on the second valvifers. The bulbi then moved in between the second valvifers, which were pushed slightly apart (Fig. 4). This movement in between the second valvifers makes the rami of the valvula/valvifer complex less curved, which might reduce the friction during the reciprocal valvulae movements. Because the ball-and-socket connection is not important during rotation of the terebra, its most likely function is stabilizing the terebra in its resting position. For further analysis of the torques acting on the system, we assume that the depression of the terebra is purely rotational around h3, ignoring the slight translation of the rotation point, which is less than the height the base.

In our reconstructions, we observed a depression of the terebra of approximately 30°, but based on high-speed video recordings of probing animals (Video S1), we expect that this can be more extreme. During terebra depression, the whole system of the basal plates rotates in the sagittal plane. This is presumably a result of the lifting and curving of the metasoma (Fig. 3), but we did not investigate the musculature responsible for these movements.

Musculature

Depression (i.e. downward rotation) of the terebra is induced by contraction of the posterior second valvifer-second valvula (P-2vlf-2vlv) muscle. This muscle inserts dorsally on the medial processus of the second valvula and fans out ventrally to the posterior part of the second valvifer (Fig. 5A,B top). The estimated maximum force generated

by this muscle is 0.381 mN (Table 2). The exact location of the rotation axis of the terebra (h3 in Fig. 1C) is difficult to determine, and we assumed this flexion point to be the thin, short rami connecting

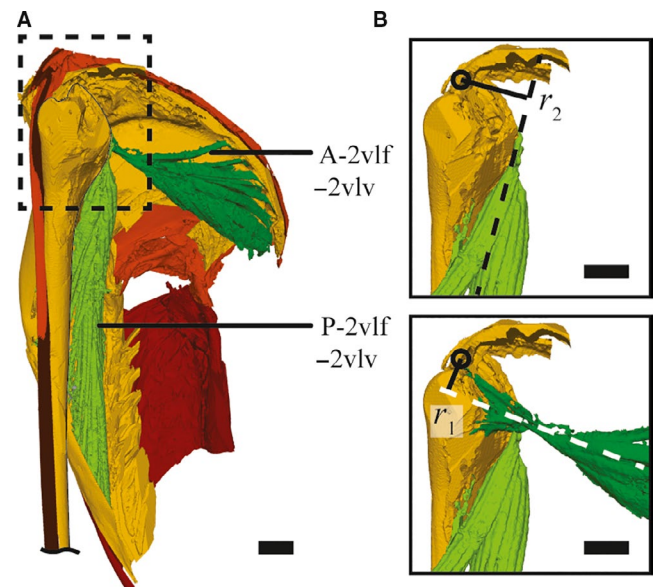








FIG. 5 Muscles that depress or elevate the terebra. Lateral view of the ovipositor apparatus in the probing position with aligned valvulae. (A) Two muscles attach directly to the anterior bulb of the second valvula. A thin line was added to outline of the second valvula to improve contrast with the second valvifer. The posterior second valvifer-second valvula (P-2vlf-2vlv) muscle connects the second valvula and the posterior end of the second valvifer and is presumably used to rotate the ovipositor towards the probing position (depression) (Fig. 8C). The anterior second valvifer-second valvula (A-2vlf-2vlv) muscle connects the second valvula to the dorsal horn of the second valvifer and is presumably used to rotate the ovipositor towards the resting position (elevation; Fig. 8F). (B) Enlarged view of the attachment sites of both muscles. Solid black lines r_1 and r_2 : moment arms of A-2vlf-2vlv and P-2vlf-2vlv respectively. Dashed lines: estimated lines of actions for both muscles. Centre of the black circles: estimated centre of rotation. For clarity, we show the high-resolution mesh of the second valvula in resting position which was fitted on the low-resolution mesh of the second valvula in probing position. Scale bars: 50 μm [Colour figure can be viewed at wileyonlinelibrary.com]

TABLE 2 Properties of the muscles associated with the ovipositor apparatus.

Muscle name (abbreviation)	Cross-section location	Position	Measured average PCSA, $\mu\text{m}^2 \times 10^3$	Corrected PCSA, $\mu\text{m}^2 \times 10^3$	Force, mN	Moment arm, μm	Torque, $\text{mN} \cdot \mu\text{m}$	
Posterior second valvifer-second valvula (P-2vlf-2vlv)		R	2.281	1.564	0.305	–	–	
		P	1.626	2.345	0.457	45.958	21.0	
Anterior second valvifer-second valvula (A-2vlf-2vlv)		R	2.657	1.355	0.264	–	–	
		P	1.445	1.418	0.277	19.466	5.38	
Medial second valvifer-second valvula (M-2vlf-2vlv)		R	0.181	0.093	0.0180	–	–	
		P	0.072	0.071	0.0139	–	–	
Dorsal T9-second valvifer (D-T9-2vlf)		R	15.04	10.318	2.01	–	–	
		P	7.432	10.714	2.09	172.921	361	
Ventral T9-second valvifer		Medial belly	R	7.964	5.462	1.07	–	–
			P	5.742	8.277	1.61	-110.406	-178
		Lateral belly (V-T9-2vlf)	R	8.697	5.965	1.16	–	–
			P	6.271	9.039	1.76	-71.891	-127
First valvifer-genital membrane (1vlf-gm)		R	0.803	0.409	0.0798	–	–	
		P	0.501	0.492	0.0959	–	–	

PCSA, physiological cross-sectional area.

Second column shows the location of the calculated PCSA (for each muscle; red line). Third column shows the animal's body position: R for resting position, P for probing position (both with aligned valvulae). The formulae used for calculating the muscle properties are provided in the Supporting Information. The force estimates reported in the main text were obtained by averaging the values of the P and R positions for each muscle.

the second valvula to the second valvifers, in between the medial and lateral processi of the second valvula base (Fig. 2C,F). The estimated moment arm of P-2vlf-2vlv muscle is 45.96 μm , which results in an estimated maximal torque of 21.0×10^{-9} Nm used to rotate the terebra into the probing position (Fig. 5B, top). Because the tendon of this muscle runs over the curved dorsal side of the valvula base, the moment arm will probably change little over the range of motion of the ovipositor.

Elevation (i.e. upward rotation) of the terebra is achieved by contraction of the anterior second valvifer-second valvula (A-2vlf-2vlv) muscle. This muscle connects the anterior inner wall of the second valvifer to the lateral processus of the second valvula (Fig. 5A,B, bottom). We estimate that the A-2vlf-2vlv muscle can provide a force of 0.270 mN (Table 2) and would, with an estimated moment arm of 19.45 μm , generate a maximal torque of 5.38×10^{-9} Nm on the terebra. Angular changes, however, have a big impact on the moment arm of this muscle, and the observed rotation. Although our observed rotation of 30° results in less than 15% reduction in torque, a rotation of 45° will result in an approximately 30% reduction in torque.

3.2.2 | Valvula motions during probing

Exoskeletal elements

As was previously shown, the valvulae move forwards and backwards relative to each other during drilling. We analysed three

distinct valvula configurations to compose a working hypothesis about the kinematics and muscle activity during probing. As previously hypothesized by others (e.g. Scudder, 1961; King, 1962; Smith, 1969; Copland, 1976), we observed that movement of the first valvulae is induced by a clear rotation of the first valvifer around its articulation with the second valvifer (h1) with changing alignment of the first and second valvulae (Figs 1C and 6). Moving the first valvulae from their complete retraction (offset $-237 \mu\text{m}$, for calculation see Supporting Information) to complete protraction (offset $\sim 121.7 \mu\text{m}$) corresponds to a rotation of the first valvifer of approximately 56° (Fig. 6, Table 3). The calculated excursion path of the first valvifer along the anterior horn of the second valvifer with this angular change is 252.6 μm , which differs slightly from the total excursion of the first valvula tip (349.7 μm ; Table 3), but is in the same order of magnitude.

According to the hypothesized mechanism, the movement of the first valvulae and first valvifers result from the translation of the second valvifer with respect to T9 (e.g. King, 1962; Copland, 1976; Fergusson, 1988; Gauld *et al.* 1988; Scudder, 2009; Eggs *et al.* 2018). This is also visible in our reconstructions (Fig. 5). The second valvifer and T9 telescopically slide away from each other when the first valvulae are retracted and vice versa when the first valvulae are protracted.

Musculature

In the following description of movement, we use the second valvifer as our reference element compared to which all movements of the

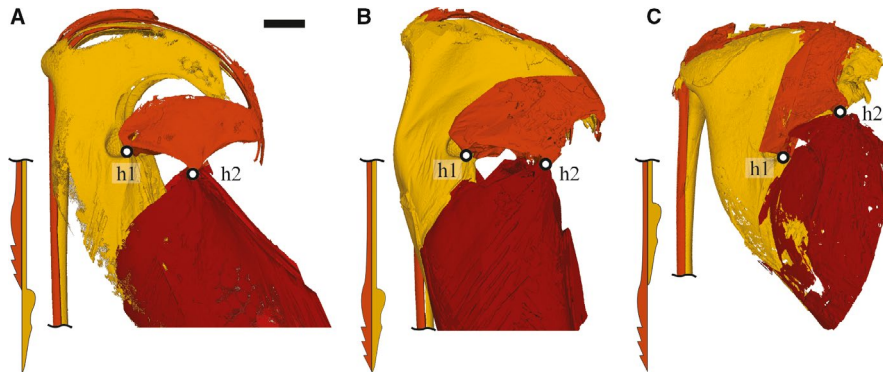





FIG. 6 Lateral view of the ovipositor apparatus in probing position with three different valvula configurations. The first valvifer (orange) changes orientation during pro- and retraction of the first valvulae. The centre of rotation is at the inter-valvifer connection hinge h1. Inserts show the relative position of the first valvulae (orange) and the second valvula (yellow). (A) First valvulae in retracted state, the first valvifers (orange) have been rotated away from the horn of the second valvifer (yellow). (B) When the valvulae are (manually) aligned, the relative positions and orientations of the valvifers are similar to the resting position with aligned valvulae. (C) When the first valvulae are (manually) protracted, the first valvifers are rotated over the horn of the second valvifers. Scale bar: 100 μm [Colour figure can be viewed at wileyonlinelibrary.com]

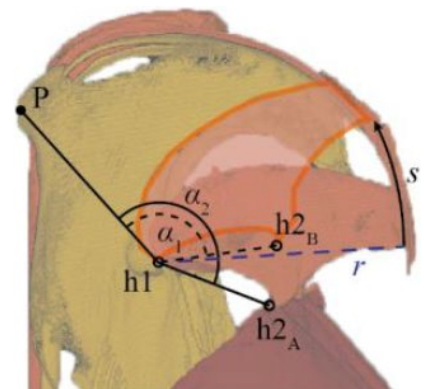
other elements are described. In reality, all elements can move relative to each other and the second valvifer does not remain stationary relative to the external frame of reference. We identified two muscles connecting the second valvifer with T9, which can actuate the sliding movements of T9 relative to the second valvifer.

Retraction of the first valvulae is achieved by contraction of the ventral T9-second valvifer muscle (V-T9-2vlf; Fig. 7A), which slides T9 posteriorly relative to the second valvifer, and increases the distance between T9 and the second valvifer horn. This results in the posterior rotation of the first valvifer around h1 due to the connection between this plate and T9 at h2. The rotation of the first valvifer moves the rami and thus retracts the first valvula. The V-T9-2vlf muscle consists of two parts, or bellies, that both originate on a medially protruding process on the anterodorsal edge of T9, but

have clearly different insertions (Fig. 2D,E, Fig. S3b). The medial muscle belly runs medial to the second valvifer and inserts on a plate on the medial side which increases the attachment area (Fig. 2D,E, Fig. S3a). The lateral belly runs in between the second valvifer and T9, and inserts on the lateral wall of the second valvifer. This muscle belly has additional fibres originating from the medial side of the T9 plate itself. The dorsal side of this part of the second valvifer has an enlarged ridge, which increases the attachment area and probably strengthens the second valvifer to oppose bending along its longitudinal axis in the dorsoventral direction. Both muscle bellies can generate comparable forces (medial: 1.34 mN, lateral: 1.46 mN; Table 2). The estimated moment arms of the muscle bellies (Fig. 7A, r3, shown only for one muscle belly) are 110.41 μm (medial) and 71.89 μm (lateral), which results in the maximal torques on the first valvifer of

TABLE 3 Movement of the first valvifers and first valvulae.

	α , $^{\circ}$	r , μm	s , μm	o , μm
First valvula retraction 	156.8	428	-	237
Aligned valvulae 	119.5	390	-	0
First valvula protraction 	101.2	396	-	121.7
Aligned to retracted ($\Delta\alpha_{\text{ret}}$)	37.3	-	262.5	
Aligned to protracted ($\Delta\alpha_{\text{prot}}$)	-18.3	-	128.4	
Full range of first valvula motion	55.6	-	390.9	358.7



The angles (α_i), radii (r_i), and excursion paths (arc lengths, s_i) were determined for all segmented probing positions and compared to the corresponding valvula offsets (o_i). The image shows the points P (reference), hinge (h)1, and h2 chosen as landmarks for calculating the angles and arc lengths in segmentations. The point h2 changes location from h2_A (first valvula retraction) to h2_B (first valvula protraction), which corresponds to the maximal change in angle $\alpha_2 - \alpha_1$. Calculation of the arc lengths and the method for determining the displacement of the valvulae are given in the Supporting Information.

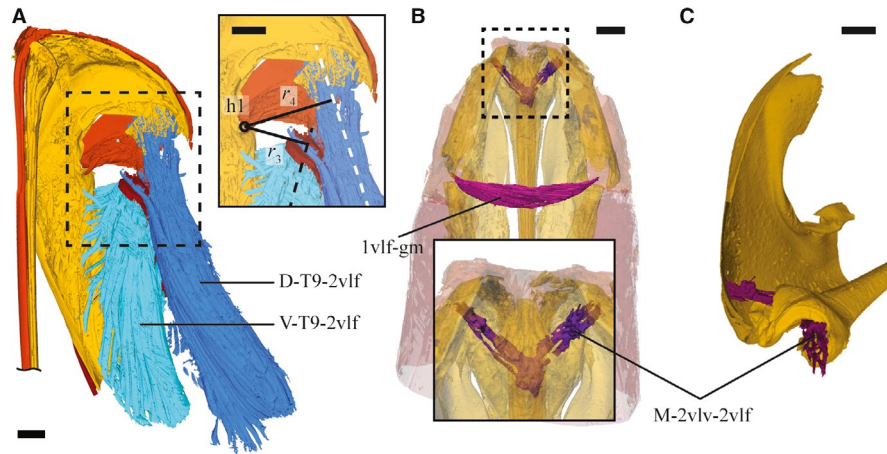


FIG. 7 Muscles actuating the reciprocal valvula movements and stabilizing the ovipositor apparatus. (A) Lateral view of the ovipositor base in the probing position. The ninth tergite (T9)-second valvifer muscle (V-T9-2vlf) muscle is fan-shaped and splits into two muscle bellies that wrap around the second valvifer. This muscle connects the anterior part of T9 with the posterior part of the second valvifer and its contraction presumably slides these two exoskeletal elements away from each other. This results in rotation of the first valvifer posteriorly, causing retraction of the first valvulae (Fig. 8E). The dorsal T9-second valvifer (D-T9-2vlf) muscle connects the dorsal horn of the second valvifer with the posterior part of T9 and its contraction slides these two exoskeletal elements towards each other. This causes rotation of the first valvifer anteriorly, leading to protraction of the first valvulae (Fig. 8D). A thin line was added to outline of the second valvula to improve contrast with the second valvifer. (B) A dorsal view of the system showing two muscles that connect its left and right sides. The first valvifer-genital membrane (1vlf-gm) muscle connects near the first valvifer-second valvifer articulation, while the medial second valvifer-second valvula (M-2vlf-2vlv) muscle (inset) links the base of the second valvula to the second valvifer. (C) Antero-medial view of the second valvula base showing the location of the M-2vlf-2vlv muscle. Scale bars: 50 μm [Colour figure can be viewed at wileyonlinelibrary.com]

178×10^{-9} Nm and 126×10^{-9} Nm (Table 2). The combined torques result in a 305×10^{-9} Nm retraction force that can be exerted on the first valvifer. In the full range of motion of the first valvifer the reduction in moment arm for this muscle is approximately 10%.

First valvifer protraction is achieved by contraction of the dorsal T9-second valvifer muscle (D-T9-2vlf), which pulls the T9 closer to the second valvifer. This induces anterior rotation of the first valvifer around h1. This, in turn, results in movement of the rami and protraction of the first valvula. The D-T9-2vlf muscle originates on the tip of the horn of the second valvifer, and runs dorsal to T9 where the muscle attaches on its posterior dorsal rim (Fig. 7A; Vilhelmsen, 2000; Vilhelmsen *et al.* 2001; Ernst *et al.* 2013). This muscle is large, with an estimated maximum force of 2.05 mN (Table 2). The estimated moment arm (Fig. 7A, r4) is $172.92 \mu\text{m}$, which leads to a maximal torque of 361×10^{-9} Nm on the first valvifer. The moment arm changes approximately 10% during the entire range of first valvifer motions, so this muscle could potentially generate very similar torques and forces throughout the probing process.

3.3 | Additional musculature associated with ovipositor apparatus

We identified two muscle groups that connect the left and the right sides of the ovipositor apparatus and which appear not to actuate the terebra. One muscle consists of only a few muscle fibres and originates on the anterior-medial (inner) wall of the second valvifer, stretches over the sides of the lateral processes of the second valvula and inserts inside the lumen of this valvula (Fig. 7B,C). As far

as we are aware, this muscle has never been described, so we did an additional histological analysis which confirmed our findings (see Supporting Information, and Fig. S2). We propose to name this muscle the medial second valvifer-second valvula muscle (M-2vlf-2vlv). This tiny muscle can exert an estimated maximal force of 0.0159 mN (Table 2). The function of this muscle is uncertain because of its location just dorsally of the rami connecting the second valvula and second valvifer; it does not seem to induce rotation, so its most probable function is stabilizing the position of the second valvifer, but other functions are possible.

Another muscle, the first valvifer-genital membrane muscle (1vlf-gm; Fig. 7B; Eggs *et al.* 2018), comprises few muscle fibres and potentially stabilizes the first valvifers with an estimated maximal force of 0.0879 mN (Table 2). The muscle originates on the medial side of the first valvifer near the hinge with the second valvifer (h1), interconnects medially, and could potentially link to the genital membrane. This membrane spans between the two ventral margins of the second valvifer dorsal to the second valvula, thus surrounding and possibly protecting the valvulae when the ovipositor is in resting position (Eggs *et al.* 2018). The membrane itself was not clearly discernible in our scans.

We also found two other muscle groups that possibly have a stabilizing function. They attach to the lateral side of the first valvifer and their muscle fibres run in a lateral direction. (Fig. S3b). These muscles are small and appear not to play an important role in actuation of the drilling mechanism. We segmented them only partially. One muscle is directed latero-posteriorly, which we denote M-1vlf-A (Fig. S3b). The other muscle (M-1vlf-B) is directed latero-ventrally towards the abdominal wall (Fig. S3b), but we could not unambiguously

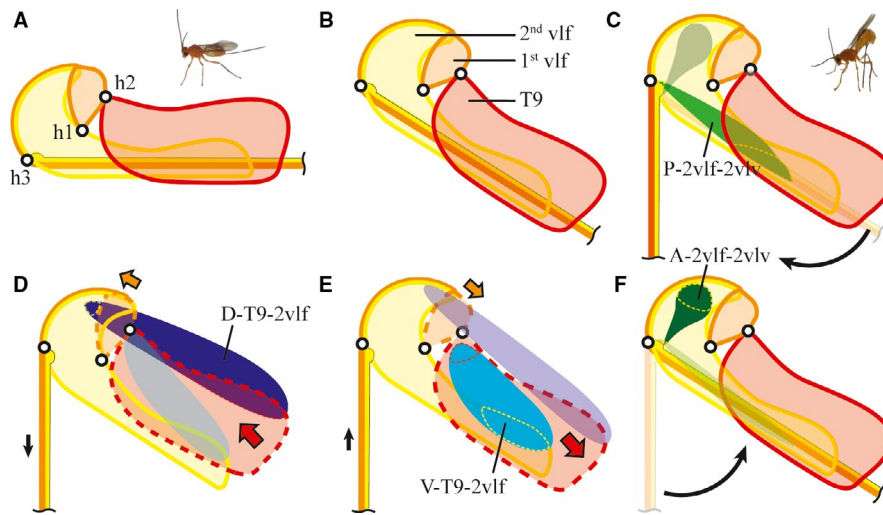


FIG. 8 Schematics of the probing mechanism in lateral view. Movements of the exoskeletal elements are shown in the reference frame of the second valvifer and are indicated with arrows. Movement is predominantly induced by the opaque muscles in each image. Muscle attachment is indicated in these muscles with a thin dotted line, in the colour of the element the muscle attaches to. (A, B) The ovipositor apparatus is rotated from the resting to probing orientation. (C) The ovipositor is depressed (i.e. downward rotation) from the metasoma using the posterior second valvifer-second valvula (P-2vlf-2vlv) muscle. (D) Contraction of the dorsal ninth tergite (T9)-second valvifer (D-T9-2vlf) muscle slides T9 towards the second valvifer, causing anterior rotation of the first valvifer and protraction of the first valvulae. (E) Contraction of the ventral T9-second valvifer (V-T9-2vlf) muscle slides T9 away from the second valvifer, causing posterior rotation of the first valvifer and retraction of the first valvulae. (F) The ovipositor is elevated (i.e. upward rotation) from the probing to resting orientation using the anterior second valvifer-second valvula (A-2vlf-2vlv) muscle. [Colour figure can be viewed at wileyonlinelibrary.com]

determine its attachment site from our scans or literature. If we assess their potential contribution to valvula movement, we must conclude that their moment arms for the described rotation points are very short. M-1vlf-A runs near the axis of rotation h2, while M-1vlf-B spans across the axis of rotation of h1 (Fig. S3b). The moment arms of these muscles do increase when the first valvulae are offset and may then contribute slightly in the actuation of the valvifer, although they probably have a stabilizing function (Imms, 1931; Fergusson, 1988).

So far, we have not mentioned the posterior T9-second valvifer muscle in this study as it was located outside of our high-resolution scanning area. We did observe this muscle in low-resolution scans of *D. longicaudata*, and it connects the T9 with the second valvifer and serves to stabilize the ovipositor during probing (Eggs *et al.* 2018).

4 | Discussion

In the present study, we analysed the actuation mechanism used in drilling with a very slender terebra in tough substrates, often used to deposit eggs in stiff substrates. A recent study showed that wasps use alternating movements of the ovipositor valvulae when penetrating the substrate (Cerkvenik *et al.* 2017). The valvula movements, which hypothetically reduce the risk of buckling damage (King and Vincent, 1995), are initiated at their bases inside the metasoma. Although the morphology of this basal ovipositor apparatus and the muscle attachments have been extensively described (e.g. Imms, 1931; King, 1962; Scudder, 1971; Smith, 1972; Copland, 1976; Eggs *et al.* 2018), no one has, as far as we are aware, quantitatively

analysed the configurational changes of the basal ovipositor apparatus that occur during probing. In the present paper, we reconstruct the movements in the ovipositor base using configurations from three distinct phases of the probing behaviour and the resting position. We also analyse the muscles that make these movements possible and estimate their maximum contraction forces. For these muscles, we describe the most obvious function when no other muscles are active. Combinations of muscle contractions or isometric contractions can lead to additional functions, but we do not consider those as we focus on clearly specified phases of the probing behaviour, which can all be explained by contractions of the muscles we discuss. Below, we describe these important phases of the probing behaviour.

4.1 | Probing mechanism

4.1.1 | Moving between resting and probing positions

Upon the start of probing, a female parasitic wasp raises its metasoma, curves it ventrally, and rotates (depresses) the terebra from its resting backward orientation to a downward orientation (Fig. 8A-C; Video S1; Le Lannic and Nénon, 1999; Kundanati and Gundiah, 2014; Cerkvenik *et al.* 2017; Eggs *et al.* 2018). From our analysis, it is clear that the entire ovipositor base rotates during the ventral curving of the metasoma (seen in high-speed videos, Video S1) as the angle between the first valvifer and T9 changes only slightly (Fig. 3). The depression of the terebra is most likely achieved by the P-2vlf-2vlv

muscle, which can pull the second valvula dorso–posteriorly and rotates the valvulae (Fig. 7C; Imms, 1931; Copland, 1976; Fergusson, 1988; Vilhelmsen, 2000; Vilhelmsen *et al.* 2001; Eggs *et al.* 2018). We could not determine the maximal rotation angle of the terebra with certainty, as this was probably affected during the fixing procedure and scanning. However, based on the reported probing process of parasitic wasps, the valvulae can rotate over a larger angle than observed here. Based on pictures taken during oviposition (Kundanati and Gundiah, 2014; Cerkvenik *et al.* 2017), we estimate that the valvulae can rotate at least up to 60° with respect to their basal plates. At the end of probing, when the animal completely extracts its terebra from the substrate, it is likely that contraction of the A-2vlf-2vlv muscle pulls on the lateral process of the second valvula anteriorly, rotating (elevating) the terebra into its resting position (Fig. 8F; Smith, King and Vincent, 1995; Quicke *et al.* 1995; Eggs *et al.* 2018).

4.1.2 | Valvula motions during probing

After puncturing the substrate, the wasps move the valvulae reciprocally during insertion. When one valvula is pushing into the substrate, the other valvula(e) in the substrate pull, to minimize the net force on the substrate and therefore to minimize the chance of buckling. This technique is called the push–pull mechanism (King and Vincent, 1995; Cerkvenik *et al.* 2017). As no musculature attaches directly to the valvulae (except one, see below) the reciprocal valvula movement can only be the result of the movements of their valvifers, as was previously proposed (King, 1962; Smith, 1969; Scudder, 1971; Copland, 1976; Austin, 1983; Fergusson, 1988; Copland and King, 2009; Eggs *et al.* 2018).

Our analysis shows that the movements of the second valvula are limited compared to the translations of the first valvulae. Although small forward motions of the second valvula cannot be excluded, the morphology limits movement relative to the second valvifer and it can therefore be assumed that the second valvula predominantly follows the movement of the metasoma. We did find, however, a previously undescribed muscle running into the second valvula and attaching to its inside, that may induce some movement of the second valvula. This is surprising, as the valvulae of Hymenoptera are always reported to be devoid of any musculature (Smith, 1972; Quicke, 2014). The newly described M-2vlf-2vlv attaches inside the base of the second valvula, but does not seem to extend deep inside the external ovipositor. The muscle is small and cannot generate high forces. The direction of the muscle fibres of M-2vlf-2vlv indicates that its contraction may pull the second valvula towards the second valvifer. This muscle can therefore pull on the second valvula and increase the tension in the valvula, contributing to the push–pull mechanism, although with little force. This muscle may also be active during terebra extraction because it can support the thin second valvula-second valvifer rami which might come under high tensile stresses during retraction of the terebra. Finally, activation of the individual left or right muscle bellies of this muscle may induce small

rotational forces on the terebra, although this seems unlikely due to the small size of the muscle.

The important backward and forward movements of the first valvulae are initiated by muscles that act on the first valvifers, which cause a rotation around h1 with the second valvifer (Fig. 1C, Fig. 6; h1). The movements of the first valvulae are probably powered indirectly by the muscles connecting the second valvifer to T9, as was also previously predicted (King, 1962; Smith, 1969; Scudder, 1971; Copland, 1976; Austin, 1983; Fergusson, 1988; Copland and King, 2009; Eggs *et al.* 2018). These muscles are large and can generate the largest torques on the valvifers (Table 2). Contraction of the D-T9-2vlf muscle causes anterior rotation of the first valvifers and protraction of the first valvulae (Fig. 7D). Contraction of the V-T9-2vlf muscle causes posterior rotation of the first valvifer and retraction of the first valvulae (Fig. 7E). These torques lead to driving forces on the first valvulae in the range of 0.874–1.19 mN, using the estimated moment arm of the first valvula scaled to the control specimen of 372.29 µm. How these forces relate to the pushing forces during substrate probing is hard to determine because they depend on many environmental factors, such as the condition of the substrate, but it is more than sufficient to pierce fruits (Leyva *et al.* 1991).

The left and right first valvifers are connected via the 1vlf-gm muscle. This muscle presumably also links to the medial genital membrane and might stabilize the overall configuration of the ovipositor base to avoid damage in the abdominal cavity (Vilhelmsen, 2000). Additionally, the 1vlf-gm muscle might contribute to bringing the first valvulae in their aligned configuration. Two other small muscles we report here also attach to the lateral side of the first valvifer (Fig. S3b). These muscles appear to have a very small effect on the rotation of the first valvifer, and are thought to only assist in moving the valvulae (King, 1962) or serve as stabilizers (Fergusson, 1988).

4.2 | Push–pull mechanism

The alternating valvula motions (push–pull mechanism) which are observed during drilling are hypothesized to reduce the risk of buckling during insertion by minimizing the net pushing forces on the terebra (King and Vincent, 1995). We can roughly estimate the critical load, or buckling threshold, of the terebra of *D. longicaudata* using Euler-Bernoulli beam bending theory, and compare this to the estimated (net) pushing force the first valvulae can exert to determine whether the terebra will buckle during probing.

The terebra contains the egg canal between and lumina within the valvulae, so we approximated it with a hollow cylinder [outer radius 15 µm, inner radius 10 µm, length 5.7 mm (Cerkvenik *et al.* 2017; King and Vincent, 1995; Leyva *et al.* 1991)]. Furthermore, we used the Young's modulus for the entire terebra of 3.60 GPa, which has been determined in this species (Cerkvenik *et al.* 2019). For simplicity of the model, we assumed that the terebra is fixed at both ends during the drilling phase; one end just inserted in the substrate, the other end inside the stationary metasoma. We are aware that buckling can be higher when the tip is not yet inserted in the substrate,

but parasitoid wasps that drill in wood seem to avoid this by targeting existing cracks (Spradbery, 1970; King and Vincent, 1995), which also helps fixing the distal end of the ovipositor before drilling (King and Vincent, 1995). Calculations for this configuration show that buckling is likely at a load of 0.140 mN (see Supporting Information for calculation). This is one magnitude smaller compared to the estimated pushing force of 1.19 mN that a single first valvula can deliver, while completely ignoring any additional forces produced by the metasoma.

However, according to the push–pull mechanisms, the pushing force of one valvula is cancelled by the pulling force on the other ones (Cerkvenik *et al.* 2017; Cerkvenik *et al.* 2019). Again, when only looking into the dynamics of the first valvulae, subtracting the pro- and retraction forces (1.19 and 0.874 mN, respectively) results in the net estimated pushing force of 0.316 mN, which is close to, but still about twice as high as the above calculated buckling threshold.

This shows that an unsupported terebra is still at risk of buckling. In reality, specialized sheaths (or third valvulae) envelop the terebra at rest and during the probing process (Vilhelmsen, 2003; Vilhelmsen and Turrisi, 2011; Cerkvenik *et al.* 2017). In *D. longicauda*, the sheaths detach only when a considerable length of the terebra (approximately 75%) has already been inserted into the substrate [Fig. S4; (Cerkvenik *et al.* 2017)]. The sheaths increase the effective terebra width and second moment of area, and therefore the load required for buckling. Already a modest twofold increase of the terebra outer radius increases the buckling threshold to 2.75 mN, more than double the pushing force that a single first valvula can deliver. This illustrates the importance of the external supporting mechanisms wasps employ during probing such as the mentioned sheaths or clamping (King and Vincent, 1995; Le Lannic and Nénon, 1999; Vilhelmsen and Turrisi, 2011; Kundanati and Gundiah, 2014).

In conclusion, the overall mechanism for terebra insertion of *D. longicauda* shows several adaptations to overcome the challenges of slender probe insertion. The semi-circular shape of the second valvifer horn, in combination with the flexible rami of the first valvifer makes depression of the terebra possible, without interfering with the actuation system. Based on our estimations, the insertion force is mostly applied by the main actuators of first valvula protraction (D-T9-2vlf). The two muscle bellies together can generate a force of approximately 2.80 mN, which leads to an estimated pushing force of 1.19 mN of each first valvula at the substrate. This is more than sufficient to pierce fruits (Leyva *et al.* 1991), in which hosts are usually found. We also show that both the push–pull mechanism (King and Vincent, 1995; Cerkvenik *et al.* 2017; Cerkvenik *et al.* 2019) and the sheaths surrounding the terebra are essential to avoid buckling, even though pushing forces applied by the first valvulae are relatively small. It also shows that the animals cannot apply high forces with the metasoma without the risk of buckling when part of the terebra is still outside the substrate.

Although a similar actuation system has been described in other wasps (e.g. Whiting, 1967; Smith, 1970; Fergusson, 1988; Copland and King, 2009; Eggs *et al.* 2018), analysis and force calculations in a wider range of species, which use different probes in different

substrates, will provide further insights into the subtle adaptations related to other life histories. In addition, a good understanding of the probing mechanism of wasps can be applied in the development of man-made probes with similar requirements as probing wasps. Thin steerable needles are an example for medical applications that can be used for hard-to-reach places in the body, and inside vulnerable tissues. A clear insight of the probing mechanism of parasitic wasps and other probing insects could therefore lead to innovations in this rapidly advancing field.


ACKNOWLEDGEMENTS

We acknowledge the Paul Scherrer Institut, Villigen, Switzerland for provision of synchrotron radiation beam time at the TOMCAT beamline X02DA of the SLS. We also acknowledge the National Institute of General Medical Sciences of the National Institutes of Health for their role in the development of the Seg3D software (grant number P41 GM103545-18) for segmentation purposes. We also thank Remco Pieters for technical support; Henk Schipper for help with sample preparations, Karen Leon-Kloosterziel for animal care, Wouter van Veen and Cees Voeseek for IT support, Kees Spoor for providing the MatLab code for calculating muscle moment arms, Florian Link for MeVisLab support, Bart Biemans for MeVisLab network ideas, and the user committee of the Netherlands Organization for Scientific Research Division Applied and Engineering Sciences (NWO TTW) WASP project and the members and students of the research group for their useful discussions. This project was financially supported by NWO/TTW grant STW12712.

DATA AVAILABILITY STATEMENT

The data that support the findings of this study are openly available in Dryad at <https://doi.org/10.5061/dryad.c2fqz6158> (van Meer, Noraly M.M.E. *et al.* (2020)).

ORCID

Noraly M. M. E. van Meer  <https://orcid.org/0000-0001-5105-0655>

Uroš Cerkvenik  <https://orcid.org/0000-0002-3761-9945>

Christian M. Schlepütz  <https://orcid.org/0000-0002-0485-2708>

Johan L. van Leeuwen  <https://orcid.org/0000-0002-4433-880X>

Sander W. S. Gussekloo  <https://orcid.org/0000-0002-9691-4661>

REFERENCES

- Austin, A.D. (1983) Morphology and mechanics of the ovipositor system of *Ceratobaeus ashmead* (Hymenoptera : Scelionidae) and related genera. *International Journal of Insect Morphology and Embryology*, 12(2–3), 139–155.
- Cerkvenik, U., van de Straat, B., Gussekloo, S.W.S. and van Leeuwen, J.L. (2017) Mechanisms of ovipositor insertion and steering of a parasitic wasp. *Proceedings of the National Academy of Sciences*, 114(37), E7822–E7831.
- Cerkvenik, U., van Leeuwen, J.L., Kovalev, A., Gorb, S.N., Matsumura, Y. and Gussekloo, S.W.S. (2019) Stiffness gradients facilitate ovipositor bending and spatial probing control in a parasitic wasp. *The Journal of Experimental Biology*, 222(9), jeb195628.

- Cerkvenik, U., Dodou, D., van Leeuwen, J.L. and Gussekloo, S.W.S. (2019) Functional principles of steerable multi-element probes in insects. *Biological Reviews*, 94(2), 555–574.
- Chapman, R.F. (2013) The abdomen, reproduction and development. In: *The insects: structure and function*. (eds Simpson, S.J. and Douglas, A.E.), 5th ed., pp. 334–342. Cambridge, MA: Cambridge University Press.
- CIBC (2016). *Seg3D: Volumetric Image Segmentation and Visualization* [Internet]. Scientific Computing and Imaging Institute (SCI). Available at: <http://www.seg3d.org>
- Cignoni, P., Callieri, M., Corsini, M., Dellepiane, M., Ganovelli, F. and Ranzuglia, G. (2008) MeshLab: an open-source mesh processing tool. In: *Sixth Eurographics Italian Chapter Conference*. (eds. Scarano, V., De Chiara, R. & Erra, U.), pp. 129–136.
- Copland, M.J.W. (1976) Female reproductive system of the Aphelinidae (Hymenoptera: Chalcidoidea). *International Journal of Insect Morphology and Embryology*, 5(3), 151–166.
- Copland, M.J.W. and King, P.E. (2009) The structure of the female reproductive system in the Torymidae (Hymenoptera: Chalcidoidea). *Transactions of the Royal Entomological Society of London*, 124(2), 191–212.
- Copland, M.J.W., King, P.E. and Hill, D.S. (2009) The structure of the female reproductive system in the Agaonidae (Chalcidoidea, Hymenoptera). *Journal of Entomology Series A, General Entomology*, 48(1), 25–35.
- Eggs, B., Birkhold, A.I., Röhrle, O. and Betz, O. (2018) Structure and function of the musculoskeletal ovipositor system of an ichneumonid wasp. *BMC Zoology*, 3(1), 12.
- Elias, L.G., Teixeira, S.P., Kjellberg, F. and Pereira, R.A.S. (2012) Diversification in the use of resources by Idarnes species: bypassing functional constraints in the fig-fig wasp interaction. *Biological Journal of the Linnean Society*, 106(1), 114–122.
- Ernst, A., Miko, I. and Deans, A. (2013) Morphology and function of the ovipositor mechanism in Ceraphronoidea (Hymenoptera, Apocrita). *Journal of Hymenoptera Research*, 1(33), 25–61.
- Evans, M.E.G. (2009) Locomotion in the Coleoptera Adephaga, especially Carabidae. *Journal of Zoology*, 181(2), 189–226.
- Fergusson, N.D.M. (1988) A comparative study of the structures of phylogenetic importance of female genitalia of the Cynipoidea (Hymenoptera). *Systematic Entomology*, 13(1), 13–30.
- Gauld, I.D., Bolton, B., Huddleston, T., Fitton, M.G., Shaw, M.R. and Noyes, J.S. et al (1988). The structure of Hymenoptera. In: *The Hymenoptera*. (eds. Gauld, I. and Bolton, B.), 56–76. Oxford: Oxford University Press, British Museum.
- Ghara, M., Kundanati, L. and Borges, R.M. (2011) Nature's Swiss Army knives: ovipositor structure mirrors ecology in a Multitrophic Fig Wasp Community. *PLoS ONE*, 6(8), e23642.
- Godfray, H.C.J. (1994) *Parasitoids: behavioral and evolutionary ecology*. Princeton, NJ: Princeton University Press, pp. 83–143.
- Goyens, J., Dirckx, J., Dierick, M., Van Hoorebeke, L. and Aerts, P. (2014) Biomechanical determinants of bite force dimorphism in *Cyclommatus metallifer* stag beetles. *Journal of Experimental Biology*, 217(7), 1065–1071.
- Heatwole, H., Davis, D.M. and Wenner, A.M. (2010) The behaviour of *Megarhyssa*, a genus of parasitic Hymenopterans (Ichneumonidae: Ephialtinae). *Z Tierpsychol*, 19(6), 652–664.
- Imms, A.D. (1931) The rise and growth of applied entomology. *Nature*, 127(3205), 512–513.
- King, P.E. (1962) The muscular structure of the ovipositor and its mode of function in *Nasonia vitripennis* (Walker) (Hymenoptera: Pteromalidae). *Proceedings of the Royal Entomological Society of London. Series A, General Entomology*, 37(10–12), 121–128.
- King, M. and Vincent, J. (1995) The mechanism of drilling by wood wasp ovipositors. *Biomimetics*, 3(4), 187–201.
- Klass, K.-D., Matushkina, N.A. and Kaidel, J. (2012) The gonangulum: a reassessment of its morphology, homology, and phylogenetic significance. *Arthropod Struct Dev*, 41(4), 373–394.
- Kundanati, L. and Gundiah, N. (2014) Biomechanics of substrate boring by fig wasps. *Journal of Experimental Biology*, 217(11), 1946–1954.
- Le Lannic, J. and Nénon, J.-P. (1999) Functional morphology of the ovipositor in *Megarhyssa atrata* (Hymenoptera, Ichneumonidae) and its penetration into wood. *Zoomorphology*, 119(2), 73–79.
- Leyva, J.L., Browning, H.W. and Gilstrap, F.E. (1991) Effect of Host Fruit Species, Size, and Color on Parasitization of *Anastrepha ludens* (Diptera: Tephritidae) by *Diachasmimorpha longicaudata* (Hymenoptera: Braconidae). *Environmental Entomology*, 20(5), 1469–1474.
- Marone, F. and Stampanoni, M. (2012) Regriding reconstruction algorithm for real-time tomographic imaging. *Journal of Synchrotron Radiation*, 19(6), 1029–1037.
- Metscher, B.D. (2009) Micro CT for comparative morphology: Simple staining methods allow high-contrast 3D imaging of diverse non-mineralized animal tissues. *BMC Physiology*, 9(1), 11.
- Paganin, D., Mayo, S.C., Gureyev, T.E., Miller, P.R. and Wilkins, S.W. (2002) Simultaneous phase and amplitude extraction from a single defocused image of a homogeneous object. *Journal of Microscopy*, 206(1), 33–40.
- Quicke, D.L.J. (1991) Ovipositor mechanics of the braconine wasp genus *Zaglyptogastra* and the ichneumonid genus *Pristomerus*. *Journal of Natural History*, 25(4), 971–977.
- Quicke, D.L.J. (2014) *The Braconid and Ichneumonid parasitoid wasps: biology, systematics, evolution and ecology*. First. Chichester, UK: John Wiley & Sons, Ltd, p. 595.
- Quicke, D.L.J. and Fitton, M.G. (1995) Ovipositor steering mechanisms in parasitic wasps of the families Gasteruptiidae and Aulacidae (Hymenoptera). *Proceedings of the Royal Society B: Biological Sciences*, 261(1360), 99–103.
- Quicke, D.L.J., Fitton, M.G., Tunstead, J.R., Ingram, S.N. and Gaitens, P.V. (1994) Ovipositor structure and relationships within the Hymenoptera, with special reference to the Ichneumonidae. *Journal of Natural History*, 28(3), 635–682.
- Quicke, D.L.J., Fitton, M.G. and Harris, J. (1995) Ovipositor steering mechanisms in braconid wasps. *Journal of Hymenoptera Research*, 4, 110–120.
- Rospars, J.-P. and Meyer-Vernet, N. (2016) Force per cross-sectional area from molecules to muscles: a general property of biological motors. *Royal Society Open Science*, 3(7), 160313.
- Sakes, A., Dodou, D. and Breedveld, P. (2016) Buckling prevention strategies in nature as inspiration for improving cutaneous instruments: a review. *Bioinspiration & Biomimetics*, 11(2), 021001.
- Scudder, G.G.E. (1961) The functional morphology and interpretation of the insect ovipositor. *Canadian Entomologist*, 93(4), 267–272.
- Scudder, G.G.E. (1971) Comparative morphology of insect genitalia. *Annual Review of Entomology*, 16(1), 379–406.
- Scudder, G.G.E. (2009) The comparative morphology of the insect ovipositor. *Transactions of the Royal Entomological Society of London*, 113(2), 25–40.
- Smith, E.L. (1969) Evolutionary morphology of external insect genitalia. 1. Origin and relationships to other appendages. *Annals of the Entomological Society of America*, 62(5), 1051–1079.
- Smith, E.L. (1970) Evolutionary morphology of the external insect genitalia. 2. Hymenoptera. *Annals of the Entomological Society of America*, 63(1), 1–27.
- Smith, E.L. (1972) Biosystematics and morphology of symphyta—III external genitalia of *Euura* (Hymenoptera: Tenthredinidae): sclerites, sensilla, musculature, development and oviposition behavior. *International Journal of Insect Morphology and Embryology*, 1(4), 321–365.
- Spradbery, J.P. (1970) Host finding by *Rhyssa persuasoria* (L.), an ichneumonid parasite of siricid woodwasps. *Animal Behaviour*, 18, 103–114.
- Stampanoni, M., Groso, A., Isenegger, A., Mikuljan, G., Chen, Q., Bertrand, A. et al (2006) Trends in synchrotron-based tomographic imaging: the SLS experience. In: Bonse, U. (Ed.) *Developments in X-Ray Tomography V*. San Diego, CA: SPIE optics + photonics., p. 63180M.

- van Meer, Noraly M.M.E., et al. (2020) Segmented volumes of the ovipositor actuation mechanism of parasitic wasp *Diachasmimorpha longicaudata*. *Dryad, Dataset*, <https://doi.org/10.5061/dryad.c2fqz6158>.
- Vilhelmsen, L. (2000) Before the wasp-waist: comparative anatomy and phylogenetic implications of the skeleto-musculature of the thoraco-abdominal boundary region in basal Hymenoptera (Insecta). *Zoomorphology*, 119(4), 185–221.
- Vilhelmsen, L. (2000) The ovipositor apparatus of basal Hymenoptera (Insecta): phylogenetic implications and functional morphology. *Zool Scr.*, 29(4), 319–345.
- Vilhelmsen, L. (2003) Flexible ovipositor sheaths in parasitoid Hymenoptera (Insecta). *Arthropod Structure & Development*, 32(2–3), 277–287.
- Vilhelmsen, L. and Turrisi, G.F. (2011) Per arborem ad astra: morphological adaptations to exploiting the woody habitat in the early evolution of Hymenoptera. *Arthropod Structure & Development*, 40(1), 2–20.
- Vilhelmsen, L., Isidoro, N., Romani, R., Basibuyuk, H.H. and Quicke, D.L.J. (2001) Host location and oviposition in a basal group of parasitic wasps: the subgenual organ, ovipositor apparatus and associated structures in the Orussidae (Hymenoptera, Insecta). *Zoomorphology*, 121(2), 63–84.
- Whiting, A.R. (1967) The biology of the parasitic wasp *Mormoniella vitripennis* [= *Nasonia brevicornis*] (Walker). *The Quarterly Review of Biology*, 42(3), 333–406.
- Yoder, M.J., Mikó, I., Seltmann, K.C., Bertone, M.A. and Deans, A.R. (2010) A gross anatomy ontology for hymenoptera. *PLoS ONE*, 5(12), e15991.
- Zeh, D.W., Zeh, J.A. and Smith, R.L. (1989) Ovipositors, amnions and egg-shell architecture in the diversification of terrestrial arthropods. *The Quarterly Review of Biology*, 64(2), 147–168.

SUPPORTING INFORMATION

Additional supporting information may be found online in the Supporting Information section.

How to cite this article: van Meer NMME, Cerkvenik U, Schlepütz CM, van Leeuwen JL, Gussekloo SWS. The ovipositor actuation mechanism of a parasitic wasp and its functional implications. *J. Anat.* 2020;237:689–703. <https://doi.org/10.1111/joa.13216>